JETIR.ORG ISSN: 2349-5162 | ESTD Year : 2014 | Monthly Issue
JOURNAL OF EMERGING TECHNOLOGIES AND INNOVATIVE RESEARCH (JETIR)
An International Scholarly Open Access, Peer-reviewed, Refereed Journal

Acid-Catalyzed Dehydrative Imination of Benzil using 2-Amino-4-chloro-5-nitrophenol, Incorporating it with Metal Ions and Exploring their Biological-Environmental Insights

Shivanshu Brahmchari* and A. P. Mishra,

Department of Chemistry, Dr. Harisingh Gour Vishwavidyalaya (A Central University), Sagar, Madhya Pradesh, India (470003).

Abstract

This work details the synthesis and comprehensive structural analysis of Co(II) and Ni(II) metal ions coordinated with the novel Schiff base ligand 6,6'-((1,2-Diphenylethane-1,2-diylidene)bis(azaneylylidene))bis(4-chloro-3-nitrophenol) (SBE), synthesized during the acid-catalyzed condensation of Benzil and 2-Amino-4-chloro-5-nitrophenol. Structural investigations were conducted using UV-Vis., FT-IR, NMR, mass spectrometry, P-XRD, thermal analysis, and DFT calculations, uncovering distinctive structural features and enhanced thermal stability of the complexes relative to the ligand SBE. Biological assessments demonstrated that the SBE ligand had a better antifungal potency, particularly against Aspergillus niger and Fusarium oxysporum, compared to its Co(II) and Ni(II) complexes, although their effectiveness was lower than that of commercial standards. On the other hand, the Ni(II) complex (SBENi) demonstrated the highest photocatalytic efficiency in degrading Methylene Blue dye. These findings underscore the varied potential of the newly synthesized Schiff base ligand and its metal complexes in catalytic and biological uses.

Key words: Imine, Schiff base, characterization, Antifungal, and Dye-degradation.

1. Introduction

Schiff base ligands and their corresponding metal complexes have attracted considerable attention in coordination chemistry due to their wide-ranging applications in catalytic, biological, and environmental fields [1-3]. These compounds are typically synthesized through the condensation of carbonyl compounds (aldehydes and ketones) with primary amines, exhibiting the azomethine (-C=N-) linkages, which act as nitrogen analogues of the parent carbonyl compounds [4]. These linkages not only facilitate coordination with metal ions but also affect their chemical reactivity and electronic properties. Notably, Schiff bases derived from aromatic ketones, such as benzil (1,2-diphenylethane-1,2-dione), a symmetrical aromatic diketone, act as valuable precursors for the synthesis of Schiff base ligands due to their extensive conjugation and ability to form rigid, planar structures upon condensation. The diketone functionality allows the formation of bis-Schiff bases, which can serve as multidentate ligands. The synthesized compounds have shown remarkable chelating capabilities when paired with aromatic amines or aminophenols, resulting in stable and often biologically active metal complexes [5,6].

Schiff base ligands, particularly those featuring halogen-substituted phenols like 2-amino-4-chloro-5-nitrophenol, introduces a unique electronic environment due to the presence of electron-donating and withdrawing groups. The halogen substitution often contributes to enhanced biological activity by influencing the ligand's electronic properties [7]. The incorporation of transition metal ions such as Co(II), and Ni(II) into the framework of azomethine-based ligands is of significant interest, as it modulates their structure, stability, and functional potential. Cobalt(II) complexes are recognized for their catalytic, magnetic, and antimicrobial properties, while nickel(II) complexes are extensively studied for their role in enzymatic mimics and electronic materials [8,9].

This study reports the acid-catalyzed synthesis of a novel Schiff base ligand, 6,6'-((1,2-Diphenylethane-1,2-diylidene)bis(azaneylylidene))bis(4-chloro-3-nitrophenol) (SBE) formed during the condensation of Benzil with 2-Amino-4-chloro-5-nitrophenol. The synthesized ligand SBE was further ligated with transition metal ions i.e., Co(II), and Ni(II), framing their metal complexes. The structural elucidation of the ligand and its metal complexes was comprehensively carried out through various physicochemical techniques, including UV-Vis, FT-IR, ^{1}H-NMR, mass spectrometry, powder X-ray diffraction (P-XRD), and thermogravimetric analysis (TGA).

To gain deeper understanding of the electronic properties and geometries of the ligand and its metal complexes, Density Functional Theory (DFT) calculations were performed utilizing the Gaussian 9 and 16 software, employing the B3LYP/6-31 G basis set for the ligand and LANL2DZ for the metal complexes[10,11]. Furthermore, the potential applications of these synthesized compounds were assessed through biological and environmental assays, encompassing antifungal, and dye-degradation studies. This research aims to

to provide comprehensive insights into the structural, electronic, and functional characteristics of the novel Schiff base ligand and its metal complexes, highlighting potential applications in the biomedical and environmental applications.

2. Experimental Details

2.1. Reagents and instruments employed:

The reagents used in present work includes 2-Amino-4-chloro-5-nitrophenol (Mol. Wt. 188.57 g/mol), Benzil (Mol. Wt. 210.23); Cobalt chloride hexahydrate ($CoCl_2 \cdot 6H_2O$, Mol. Wt. 237.93 g/mol), Nickel chloride hexahydrate ($NiCl_2 \cdot 6H_2O$, Mol. Wt. 237.69 g/mol), Ethanol (Mol. Wt. 46.07 g/mol), Methanol (Mol. Wt. 32.04 g/mol), Diethyl ether (Mol. Wt. 74.12 g/mol), Chloroform (Mol. Wt. 119.38 g/mol), Acetic acid (60.05 g/mol) and Dimethyl Sulfoxide(DMSO) (Mol. Wt. 78.13 g/mol), all of analytical grade, procured from Sigma-Aldrich, TCI, CDH, India.

The synthesized compounds were extensively characterized through various analytical techniques. FT-IR spectra were recorded on a BRUKER Alpha-II scientific FT-IR (4000-400 cm^{-1}) instrument. UV-Vis. spectra were recorded using a LABINDIA analytical UV-3092 UV-Vis. spectrophotometer. To examine the hydrogen framework, a Bruker Avance III 500 MHz NMR spectrophotometer was utilized. Mass spectra were obtained using the WATER'S Corporation Model-Maldi-TOF Synapt XS HD Mass Spectrophotometer. P-XRD patterns of the synthesized compounds were obtained from Brucker D-8 Advanced X-ray diffractometer. Thermal analyses were carried out in static air utilizing the SDT 650 TA instrument, with a heating rate of 10°C/min. Theoretical studies (DFT calculations) were performed through Gaussian 16 W and Gaussian 9 with Gauss View 6.0 software.

2.2. Synthetic procedure for the ligand and its metal complexes

2.2.1. Synthesis of ligand SBE

The novel Benzil-derived Schiff base ligand 6,6'-((1,2-diphenylethane-1,2-diylidene)bis(azaneylylidene))bis(4-chloro-3-nitrophenol) (SBE), was synthesized reflux-assisted condensation method. In this procedure, Benzil (2 mmol, 0.4204 g) was dissolved in 35 mL of methanol, and 2-amino-4-chloro-5-nitrophenol (4 mmol, 0.7542 g) was dissolved separately in 40 mL of methanol. The two solutions were mixed in the presence of acid(acetic acid) as a catalyst, and the mixture was refluxed for 47 hours at a temperature of 70–75°C in a round-bottom flask (**Figure 1**). The reaction progress was monitored using thin-layer chromatography (TLC). After completion, the obtained wine red colored solution was cooled at room temperature, filtered and washed with methanol and kept for drying by slow evaporation. After few days, a dark red colored powder was obtained, which was washed with Methanol and recrystallized(repeated twice). A blackish red colored powder was obtained as the final product.

Mol. Formula: $C_{26}H_{16}Cl_2N_4O_6$; Mol. Wt.: 551.336; Yield: 80 %; Color: Blackish-red, M.P.: 275 ºC; stable; soluble in DMSO and partially soluble in H_2O, MeOH, EtOH, $CHCl_3$

2.2.2. Synthesis of SBE-Metal complex.

Reflux method: to synthesize metal complexes, 0.25 mmol of hydrated metal chloride $(MCl_2) \cdot nH_2O$, where M = Co(II), and Ni(II), was dissolved methanol, i.e., methanolic solution of 0.25 mmol(0.05948 g) of Cobalt chloride hexahydrate was mixed with a methanolic solution of the Schiff base ligand (SBE) (0.1378 g, 0.25 mmol); a few drops of very dilute methanolic NaOH solution was added. The reaction mixture was refluxed with continuous stirring for 5-6 h at 70-75 °C (**Figure 1**). After completion, the resulting solid powder was filtered and kept for drying by slow evaporation. Within a few days, a color powder (**Table 1**) was obtained, which was washed with Methanol and ether and kept for recrystallization (repeated twice) to yield purified desired product [12].

Solubility: The synthesized metal complexes (SBECo, and SBENi) were found to be soluble in DMSO and sparingly soluble in MeOH, EtOH, $CHCl_3$, and H_2O.

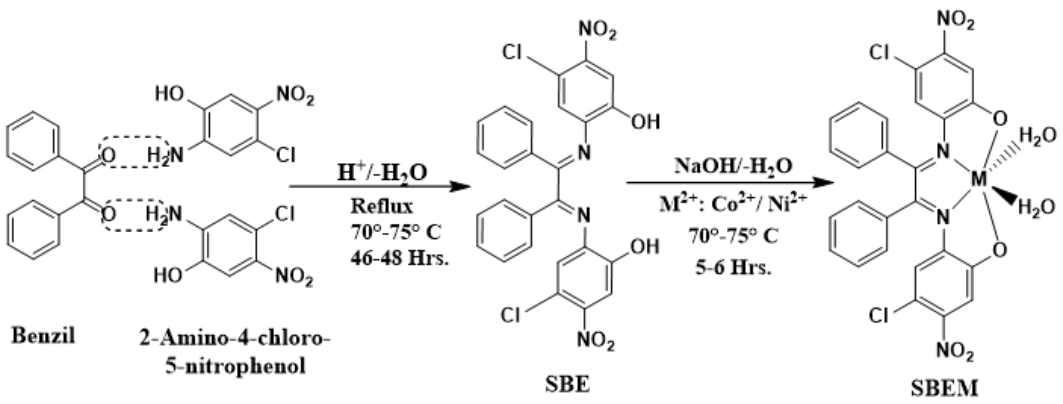

Figure 1: Synthesis of ligand SBE and its Co(II), and Ni(II) complexes and their proposed structures.

Table 1: General information about SBE ligand and its metal complexes.

Mol. formula	Sample	Mol. Wt.	Yield (%)	Color	M.P./dec (°C)	λ_m ($cm^2\Omega^{-1}mol^{-1}$)
$C_{26}H_{16}Cl_2N_4O_6$	SBE	551.336	80	Blackish-red	275	0.027
$C_{26}H_{18}Cl_2CoN_4O_8$	SBECo	644.283	79	Reddish brown	>330	0.330
$C_{26}H_{18}Cl_2NiN4_4O_8$	SBENi	644.043	74	Brown	>330	0.400

2.3. Computational Methodology for DFT calculations

To investigate the theoretical aspects of synthesized Schiff base ligand(SBE) and its metal complexes, computational calculations at density functional theory (DFT) calculations were performed, using the B3LYP functional within the Gaussian 16W and Gaussian 09 computational packages, along with Gauss View 6.0 software at 6-31G and LANL2DZ basis sets. To explore the morphologies, HUMO-LUMO, and global reactivity descriptors. The basis set B3LYP/6-31G was applied for the organic ligand(SBE), while, B3LYP/LANL2DZ was employed in case of metal complexes (SBECo, and SBENi)[13].

2.3.1. Potential Applications of Synthesized Compounds

Schiff bases and their metal complexes exhibit a diverse biological and catalytic properties, drawing the considerable interest from researchers. Some of the key applications of these compounds are discussed below:

2.3.2. Experimental Protocol for Evaluating Antimicrobial Activity

The antifungal potential of the synthesized compounds was investigated using the poison food technique (growth inhibition technique), against fungal strains; Aspergillus niger and Fusarium oxysporum [14]. Malt Extract Agar(MEA) (36g/L)media was sterilized by autoclaving and poured into petri dishes within a laminar flow chamber [14]. DMSO and water served as negative controls under identical conditions. Each fungal strain was tested in triplicate. The antimicrobial activities of each compound were then calculated as the mean of these three replicates

2.4.3 Photocatalytic Dye Degradation Assay

The dye degradation efficiency of the synthesized Schiff base ligand and its metal complexes was tested using methylene blue (MB), as a model pollutant [15,16]. A 10ppm(10 mg/L) aqueous stock solution of MB was prepared, to which 2 mg of each compound was added individually, followed by thorough mixing. The solutions were then exposed to long-wavelength UV light (365 nm), and the absorbance at 664 nm (λ_{max} of MB) was recorded at 20-minute intervals using UV-Visible spectrophotometer to monitor degradation process [17-19]. Control experiments were also conducted in absence of both the catalysts and UV light to differentiate between photolytic degradation and adsorption. The catalytic performance of each compound was quantified by calculating percentage degradation using the formula:

Percentage Degradation = $[(A_o - A_t) / A_o] \times 100$ %,

where A_o is the initial absorbance and A_t is the absorbance at a specified time point. This approach provided a quantitative evaluation of the photocatalytic and adsorptive properties of the synthesized compounds in the degradation of methylene blue.

3. Results and Discussion

3.1. Electronic Transition Analysis via UV-Vis Spectroscopy

The UV-Vis. spectra of the Schiff base ligand SBE and its metal complexes (Co(II), and Ni(II)) in DMSO illustrated significant insights into their electronic and coordination behaviour. The un-complexed ligand SBE exhibited two distinct absorption bands at ≈ 324 nm, attributed to π-π* transition of the azomethine group and a band at 515 nm corresponding to n-π* transition, that confirms the presence of lone pairs on the ligand. Upon complexation with Co(II) and Ni(II) metal ions, both π-π* and n-π* transitions exhibited a significant red shift, indicating an alteration in the electronic environment of the ligand upon complexation. Crucially, weak d-d transitions was also observed in metal complexes, providing evidence for the coordination of metal ions to SBE ligand. Specifically, The presence of d-d transitions in Co(II) at 576 nm, and 642 nm, attributed to $T_1g \rightarrow T_1g_{(P)}$ (17361.111 cm^{-1}), $T_1g \rightarrow A_2g_{(F)}$ (15576.324cm^{-1}); in Ni(II) at 595 nm, 669 nm, and 698 nm, resembling to $A_2g_{(F)} \rightarrow T_2g_{(F)}$(16,806.723 cm^{-1}), $A_2g_{(F)} \rightarrow T_1g_{(F)}$ (14,947.683 cm^{-1}) and $A_2g_{(F)} \rightarrow T_1g_{(P)}$ (14,326.647 cm^{-1}); confirms strong interaction of the SBE ligand with the metal ion [20], as shown in **Table 2** and **Figure 2**.

Table 2: Electronic Absorption Parameters of SBE and Its Metal Complexes

Samples	π-π* (nm)	n-π* (nm)	d-d (nm)
SBE	324	515	-
SBECo	340	531	576, 642 $T_1g \rightarrow T_1g_{(P)}$, $T_1g \rightarrow A_2g_{(F)}$
SBENi	333	530	595, 669, 698 ($A_2g_{(F)} \rightarrow T_2g_{(F)}$, $A_2g_{(F)} \rightarrow T_1g_{(F)}$, and $A_2g_{(F)} \rightarrow T_1g_{(P)}$)

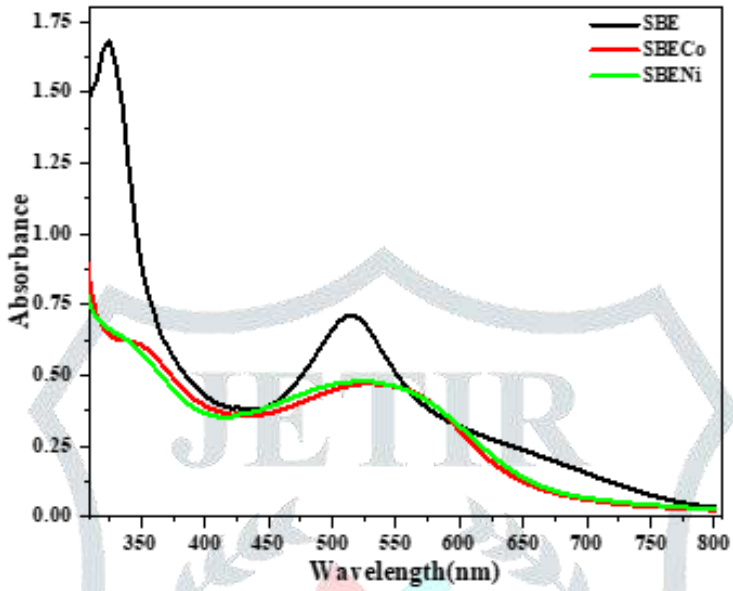

Figure 2: UV-Vis Absorbance Profiles of ligand SBE and Its Metal Complexes.

3.2. Functional Group Analysis via FT-IR Spectroscopy

The FT-IR spectra of the synthesized compounds were recorded to investigate their bonding modes. The obtained FT-IR spectrum and its data are shown in **Figure 3** and **Table 3**. The SBE ligand displayed characteristic stretching vibration at various stretching frequencies, i.e., 3382 cm^{-1}, 1664 cm^{-1}, 1563 cm^{-1}, 1408 cm^{-1}, and 1242 cm^{-1} assigned to O-H, C=N, NO, C-N, and C-O groups. Upon complexation with metal ions, the peaks were found to be downshifted, i.e., 3347-3338 cm^{-1}, 1653-1637 cm^{-1}, 1548-1537 cm-1, 1405-1395 cm^{-1}, and 1237-1215 cm^{-1}, resembling O-H (H2O), C=N, NO, C-N, and C-O groups. Furthermore, new peaks emerged in the far IR region for all metal complexes, which are characteristic of metal-ligand vibrations. The presence of these peaks in 510-509 cm^{-1} region confirms the presence of Metal-N bonding, thus demonstrating the coordination of the metal ion to the ligand [21].

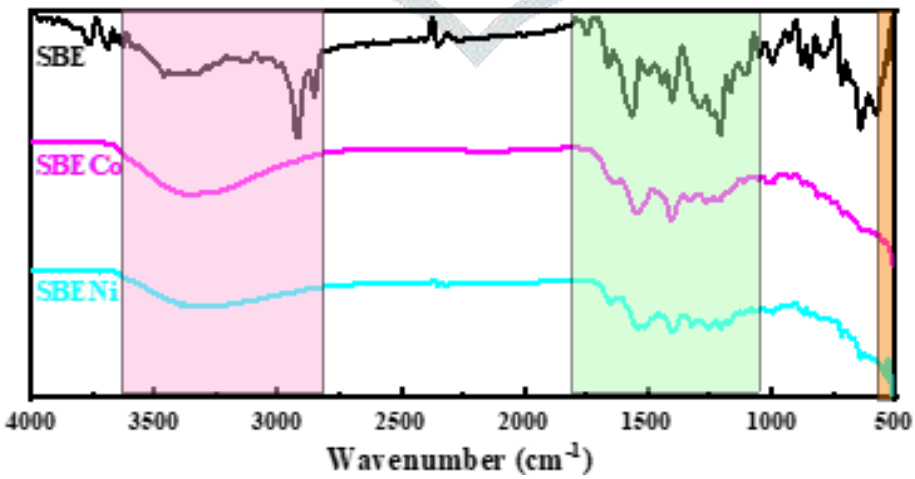

Figure 3. FT-IR analysis for SBE its Metal (Co(II) & Ni(II)) complexes in the range 4000-500 cm^{-1}.

Table 3: FT-IR Spectral Data (cm^{-1}) for SBE and Its Metal Complexes (SBECo, SBENi)

Assignments	Wavenumbers(cm^{-1})		
	SBE	SBECo	SBENi
O-H	3382	3347	3338
C=N	1664	1637	1653
NO	1563	1548	1537
C-N	1408	1405	1395
C-O	1242	1237	1215
M-N	-	509	510

3.3. Structural Elucidation via ^{1}H-NMR Spectroscopy

The structural integrity of the ligand SBE was corroborated through ^{1}H-NMR spectroscopy. The ^{1}H-NMR(500MHz, DMSO-d_6) spectrum of the ligand SBE indicated characteristic peaks/ signals for the present aromatic protons, including a signal (f) at δ_{ppm} 10.30 (s, 2H) resembling the phenolic(O-H) proton and various signals including 6.69(s, 2H), 7.49 (s, 2H), 7.64 (dd, J=7.75 Hz, 4H), 7.81 (dd, J=7.8 Hz, 2H), and 7.93 (d, J=7.4 Hz, 4H) (signal (a)-(e)) confirms the presence of various distinct aromatic protons within the ligand, as shown in the **Figure 4** [22-24].

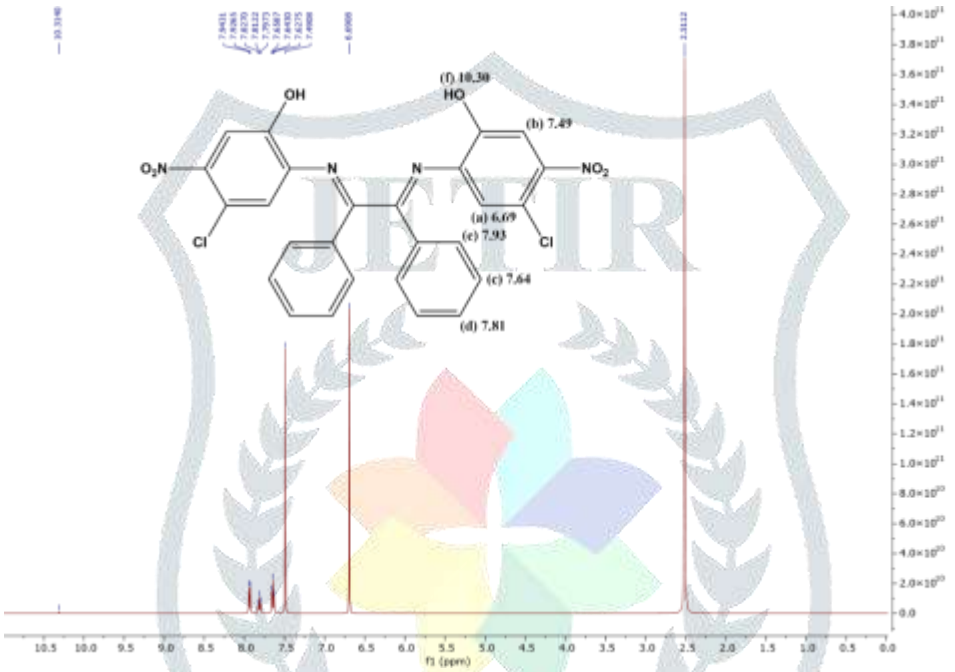

Figure 4: ^{1}H-NMR spectrum for the ligand SBE.

3.4. Molecular Mass Determination by Mass Spectrometry

Electrospray Ionization Mass Spectrometry (ESI-MS) was employed to confirm the successful synthesis and structural integrity of both the SBE ligand and its Co(II) and Ni(II) metal complexes. The ESI-MS spectra provided molecular ion peaks, with experimental mass-to-charge (m/z) ratios showing excellent agreement with theoretically calculated molecular weights. For the ligand SBE ($C_{26}H_{16}Cl_2N_4O_6$), a peak at m/z of 550.514 was noted, closely aligning with the calculated value of 550.044. Similarly, the metal complexes SBECo ($C_{26}H_{18}N_4O_8Cl_2Co$), and SBENi ($C_{26}H_{18}N4_4O_8Cl_2Ni$) exhibited experimental m/z values of 642.983, and 641.985, respectively, which were in strong agreement with their calculated values of 642.683, and 641.131. This compelling agreement between the experimental and theoretical m/z values provides substantial evidence for the successful formation, purity and corroborates the proposed molecular structures of the synthesized compounds [25].

3.5. Thermal Stability and Decomposition Analysis via TGA and DSC

Thermal studies of the synthesized ligand(SBE) and its metal complexes were performed to analyse the thermal stability and to identify the presence of water molecules both coordinated and non-coordinated [26,27]. The TG curves illustrating thermal analysis data for the ligand SBE and its Co(II)and Ni(II) metal complexes is represented in **Table 4**, demonstrating the stability of the synthesized compounds, presence of water molecules, and their step wise thermal degradation of these compounds. For all SBE-metal complexes, the initial weight loss, distinguished in the TG curves, corresponds to the evaporation of absorbed moisture. Followed by, a distinct weight loss attributed to the removal of two water molecules directly coordinated to the metal ions, confirming their presence within the coordination sphere. In contrast to the metal complexes, the ligand SBE exhibited lower thermal stability. Its thermogram (**Figure 5**) shows a rapid degradation between 220-622 ºC, specifying a sudden decomposition at higher temperatures. Conversely, the metal complexes displayed a slower, more gradual degradation profile, signifying enhanced thermal stability compared to the uncomplexed ligand (**Figure 6 & 7**). Quantitatively, the SBE ligand underwent approximately 82% thermal degradation within the studied temperature range of 30-700 ºC, whereas the metal complexes showed significantly less degradation, typically below 50%. The final residues remaining after heating were identified as char (solid carbonaceous residue) and metal oxides. These findings collectively highlight the increased thermal robustness imparted to the ligand upon complexation with the metal ions

Table 4: Thermal decomposition steps of synthesized ligand SBE and its chelated metal complexes

Sample	Temp. range (°C)	Wt. loss (%)		Assignments	Residue
		stimated	alculated		
SBE	83-220	31.85	32.81	Loss of lattice H_2O, Cl_2, $2NO_2$	Char/ carbonaceous material left
	220-308	33.42	33.05	Loss of CO, and $C_{12}H_{10}$	
	308-622	15.0	16.34	Loss of $C_5H_2N_2$	
	622-694	5.67	4.7	Loss Of C_2H_2	
SBECo	30-92	7.94	7.94	Loss of lattice H_2O	$CoO + N_2$ +Char/ carbonaceous material left
	92-150	7.76	5.29	Loss of 2 H_2O	
	150-249	13.19	1347	Loss of $2NO_2$	
	249-621	24.30	25.28	Loss of $C_8H_5Cl_2$	
	621-695	2.13	2.06	Loss of CH_2	
SBENi	30-91	4.29	4.02	Loss of lattice H_2O	$NiO + N_2$ + Char/ carbonaceous material left
	91-165	13.67	12.22	Loss of 2 H_2O, NO_2	
	165-343	13.27	17.42	Loss of NO_2, Cl_2	
	343-631	16.13	15.19	Loss of C_8H_5	
	631-692	2.59	3.88	Loss of C_2H_2	

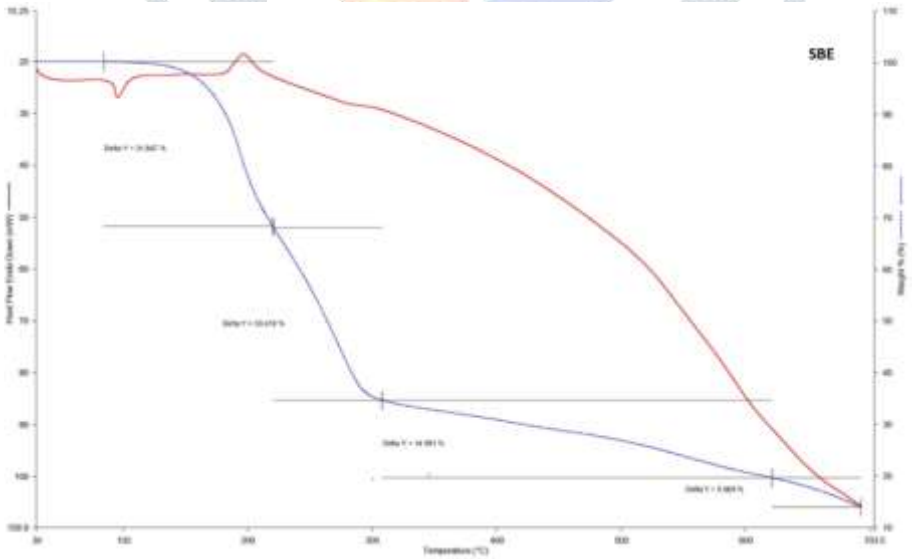

Figure 5: Thermogram for the ligand SBE.

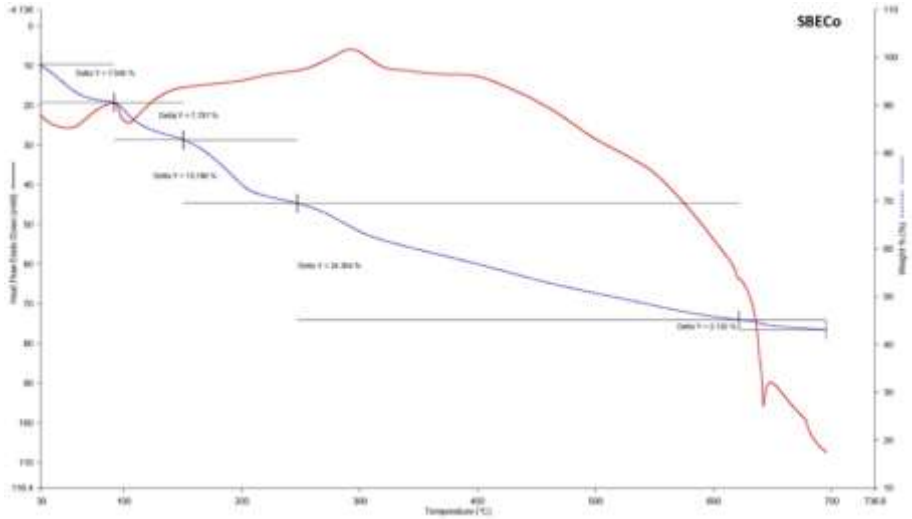

Figure 6: Thermogram for SBECo metal complex.

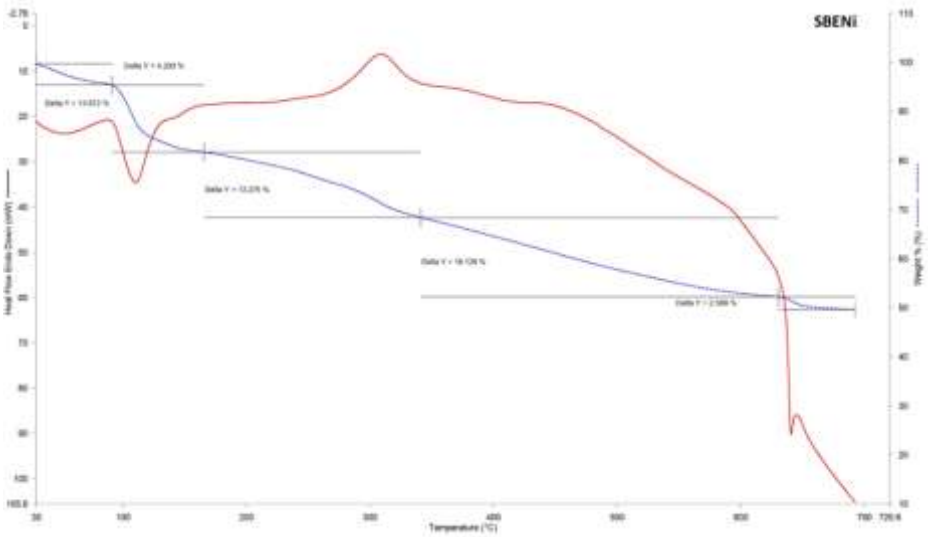

Figure 7: Thermogram for SBENi metal complex.

The DSC curves (**Figure 5-7**) illustrates insights into the thermal events, both exothermic and endothermic processes, that occur during degradation of the ligand and the metal complexes, A prominent endothermic peak was observed within the 100-200 °C range for both the ligand and Co(II) and Ni(II) complexes. In case of metal complexes, this endotherm signifies dehydration, indicating the loss of water molecules. In case of the ligand(SBE), this endothermic event, primarily indicate the sudden degradation of the ligand.

3.6. Powder X-Ray Diffraction Analysis:

Efforts to prepare single crystals of the synthesized compounds were not successful. Therefore, Powder X-Ray Diffraction (P-XRD) patterns of the synthesized ligand SBE and its metal complexes (SBECo and SBENi) were obtained within the 2θ range of 5°–80° at a scan rate of 5° per minute (**Figure 8**) to determine the crystallite size and the nature of lattice strain (compressive or tensile) in these compounds. The crystallite size of the synthesized compounds was calculated using the Scherrer equation, $D = K\lambda/\beta\cos\theta$, where K = 0.9, D is the crystallite size (nm), λ is the wavelength, and β is the full-width at half maximum (FWHM). Similarly, the Williamson-Hall equation, $\beta\cos\theta/\lambda = 1/D + \eta\sin\theta/\lambda$ (where β is the FWHM, θ is the diffraction angle, λ is the X-ray wavelength, D is the effective crystallite size, and η is the effective strain) was used to analyze the lattice strain (tensile or compressive), calculated as the slope of the plot of $\beta\cos\theta/\lambda$ versus $\sin\theta/\lambda$.

The results indicate that the particle arrangement of the solid material is irregular, suggesting interfacial characteristics between crystalline and amorphous phases [28,29], as shown in **Figure 8**. The substituted complexes displayed consistent major diffraction peaks around 2θ values of 18°, 26°, 32°, and 45°. Although the peak positions were similar among the complexes, differences were observed in their intensities and average crystallite sizes. In contrast, the ligand SBE showed distinct peak patterns, with prominent peaks at lower 2θ values (approximately 16°, 22°, 26°, 28°, 30°, and 29°), indicating a different crystal structure or arrangement compared to its metal complexes.

The calculated average crystallite sizes and lattice strain data is summarized in **Table 5**. Analysis of the Williamson-Hall plots revealed a clear difference in lattice strain. The ligand SBE exhibited tensile lattice strain, with an average strain of -2.08%. As shown in **Figure 9** (and supported by **Table 5**), this corresponds to its unique PXRD pattern and calculated strain value. Conversely, the metal complexes SBECo and SBENi exhibited both tensile and compressive lattice strain, with average strains of +1.29% and -13.87%, respectively. This indicates that the coordination with different metal ions significantly affects the lattice parameters and internal stress within the complexes, leading to varying degrees of tensile and compressive strain, which are reflected in the broadening and shifting of their PXRD peaks. The average crystallite sizes also varied, with SBECo having the largest size at 51.62 nm, followed by SBENi at 34.36 nm, and SBE being the smallest at 26.10 nm.

Table 5: Average crystallite size(nm), average strain and lattice strain of synthesized compounds.

Sample	Average Crystallite Size(nm)	Average strain (%)	Lattice strain
SBE	26.10	-2.08	Compressive
SBECo	51.62	+1.29	Tensile
SBENi	34.36	-13.87	Compressive

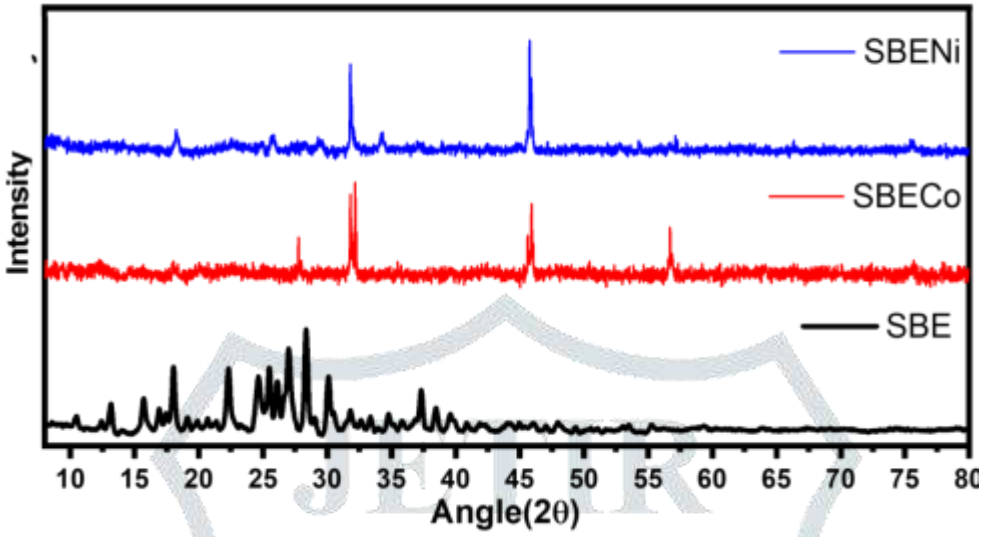

Figure 8: P-XRD spectrum for the ligand SBE and its associated SBECo, and SBENi metal complexes.

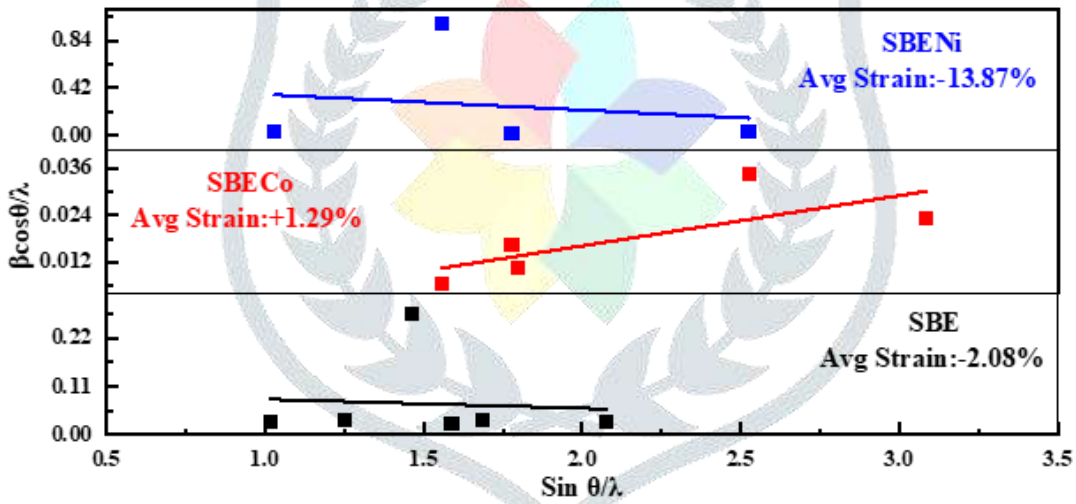

Figure 9: Plot of βcosθ/λ against sinθ/λ for SBE and its metal complexes representing their average lattice strain(nature)

3.7. Theoretical Insights through DFT-Based Computational Analysis

3.7.1. Energetic stability and Structural reorganization of Optimized Geometries

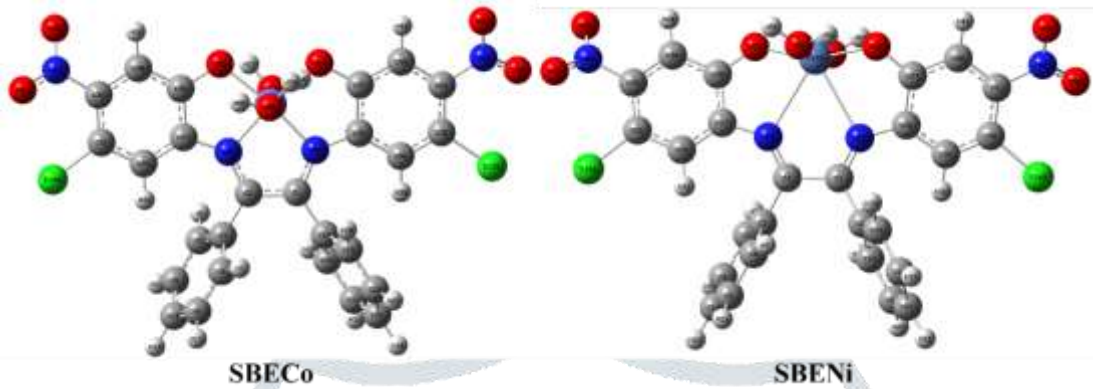

Figure 10: Optimized molecular geometry of SBE, SBECo, and SBENi with their atom number.

The structural and computational analysis of the synthesized Schiff base ligand (SBE) and its Co(II) and Ni(II) metal complexes revealed significant changes upon complexation. Geometry optimizations were performed in the gas phase using Gaussian 16W, applying the B3LYP/6-31G level for the free ligand and LANL2DZ for the metal complexes. The calculated minimum energies confirmed their structural stability, with values of -2590.355 Hartree for SBE, -1996.966 Hartree for SBECo, -2021.149 Hartree for SBENi.

Coordination of the SBE ligand to metal ions led to noticeable structural reorganizations, particularly at the ligating sites. The changes observed in bond length and bond angles upon complexation of the ligand with metal ions acts as a key evidence of metal-ligand interactions. The elongation observed in the C=N (C1=N25) bond upon complexation of the ligand to metal ions in the order: SBE < SBENi < SBECo—confesses the shifting of the electron density from imine nitrogen of the ligand towards the metal ions, and reduction of double-bond character. Similarly, the systematic change seen in other bonds such as, C28-O52; N25M59; and O52-M59 in order: SBE > SBECo > SBENi; SBENi > SBECo; and SBECo > SBENi as discussed in **Table 6,** reveals the association of the metal ions with the ligand.

The angular alterations such as in, C2–N25–M59 (SBECo > SBENi); 52-M59-O55 (SBECo > SBENi); and C1–C2–N25 (SBENi > SBE > SBECo) linkages reflects the adjustments in coordination geometries. These observations, supported by **Figure 10** and **Table 7,** resemble to the optimized geometries of the synthesized compounds and also confirm the successful complex formation.

3.7.1. Evaluation of Electron Density via Mulliken Population Analysis

The insights to the electron density distribution in SBE and its metal complexes is well fetched by the Mulliken charges data as mentioned in **Table 8,** illustrating the electron density redistribution upon complex formation. The negative charge on N25(-0.420) and O52(-0.621) atoms indicates the strong electron donation potential and the nexus sites of the ligand to the metal ions. Upon complexation, a significant change was seen over these sites i.e., N25(-0.315) and O52(-0.447) in SBECo and N25(-0.029) and O52(-0.513) in SBENi metal complexes. Correspondingly, the metals acquired positive Mulliken charges viz, Co (0.242), and Ni (0.548), supports the charge transfer mechanism.

Table 6: Bond length(nm) between some selected atoms from optimized geometries of SBE, SBECo, and SBENi.

Bond length	SBE	SBECo	SBENi
C1-C2	1.519	1.437	1.515
C1-N25	1.291	1.364	1.301
C28-O52	1.390	1.375	1.348
O52-H54	0.976	-	-
C33-N46	1.459	1.471	1.477
C27-N25	1.393	1.396	1.396
C31-Cl44	1.811	1.809	1.811
N25-M59	-	1.894	2.640
O52-M59	-	1.915	1.888
O55-M59	-	1.949	1.953

Table 7: Some selected Bond angles in SBE, SBECo, and SBENi.

Bond angle	SBE	SBECo	SBENi
C1-C2-N25	114.577	114.57	115.504
C28-O52-H54	112.375	-	-
C2-N25-M59	-	112.647	123.943
C2-N25-C27	128.691	134.42	131.936

C27-N25-M59	-	112.808	13.871
C28-O52-M59	-	109.466	125.74
O52-M59-O55	-	90.465	83.368
O55-M59-O53	-	169.244	165.328
O52-M59-O43	-	101.06	159.732
N25-M59-N26	-	85.51	60.131

Table 8: Mulliken charges of some selected atoms of SBE, SBECo, and SBENi.

Mulliken charges	SBE	SBECo	SBENi
C2	0.073	0.172	0.029
N25	-0.420	-0.315	-0.029
C27	0.197	0.252	0.041
C28	0.287	0.182	0.260
O52	-0.621	-0.447	-0.513
H54	0.389	-	-
M59	-	0.242	0.548
O55	-	-0.610	-0.679
N46	0.029	0.041	0.038
Cl44	0.175	0.001	-0.008

3.7.2. Evaluation of Global reactivity parameters

The frontier molecular orbitals—HOMO and LUMO, play a crucial role in determining a molecule's reactivity and electronic behaviour. HOMO acts as an electron donor, while LUMO serves as an electron acceptor, and hence, responsible for the reactivity and electronic properties of a compound[30,31]. The difference in energies of HOMO and LUMO are directly related to several global reactivity descriptors i.e., energy gap(ΔE), ionization potential(IP), electron affinity(EA), electronegativity(χ), chemical potential(μ), chemical hardness(η), chemical softness(σ), electrophilicity index(ω) and nucleophilicity index(ε). These descriptors can be calculated using Koopmans' theorem[32], and are summarized in **Table 9**.

According to Koopmans' theorem:

$$\text{Ionization potential (IP)} = -(E_{HOMO})$$

$$\text{Electron affinity (EA)} = -(E_{LUMO})$$

$$\text{Electronegativity } (\chi) = (IP + EA) / 2$$

$$\text{Chemical potential}(\mu) = (E_{HOMO} + E_{LUMO}) / 2$$

$$\text{Chemical hardness } (\eta) = (IP - EA) / 2$$

$$\text{Chemical softness } (\sigma) = 1/\eta$$

$$\text{Electrophilicity index } (\omega) = \mu^2 / 2\eta$$

$$\text{Nucleophilicity index } (\varepsilon) = 1/\omega$$

These descriptors offer a comprehensive understanding of the electronic structure and reactive tendencies of the ligand and its metal complexes [33].

Table 9: Global reactivity parameters of the ligand SBE and its SBECo & SBENi metal complexes

Parameters	SBE	SBECo	SBENi
HOMO Energy(eV)	-6.4815	-5.4491	-6.0709
LUMO Energy(eV)	-3.0474	-3.4033	-3.5418
$\Delta E=(E_{LUMO}-E_{HOMO})$ (eV)	3.4341	2.0458	2.5291
IP	6.4815	5.4491	6.0709
EA	3.0474	3.4033	3.5418
χ	4.7644	4.4262	4.8063

μ	-4.7644	-4.4262	-4.8063
η	1.717	1.0229	1.2645
σ	0.5824	0.9776	0.7907
ω	6.6101	9.5763	9.1340
ε	0.1512	0.1044	0.1095
Dipole moment (Debye)	12.0327	9.3463	4.9128

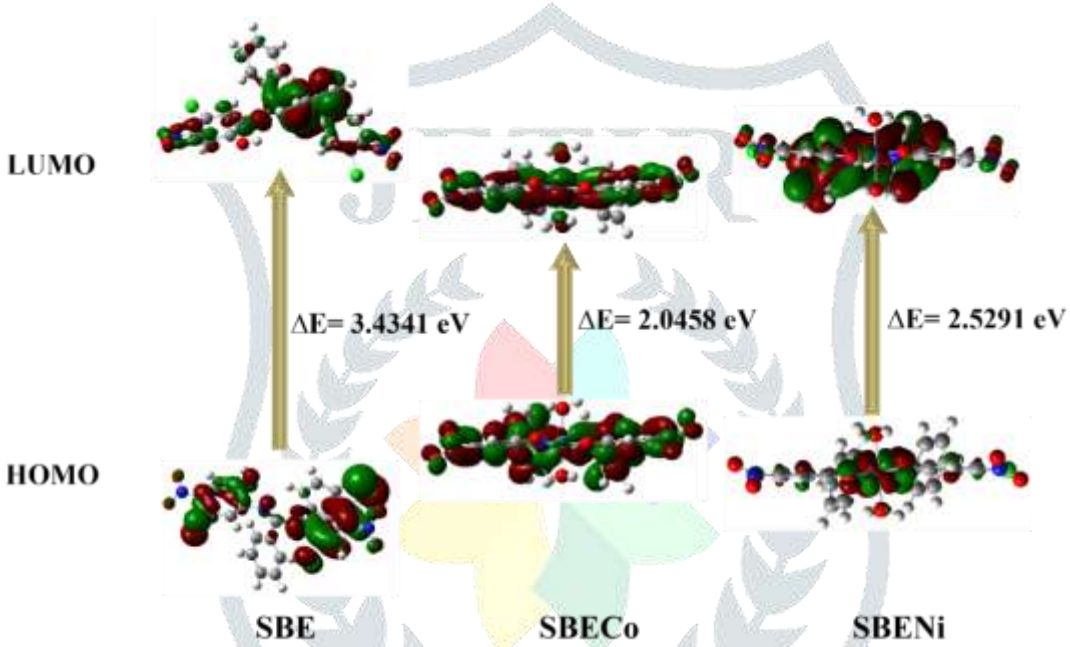

Figure 11: HUMO – LUMO orbitals of the ligand SBE and its metal complexes SBECo, and SBENi.

The energy gap corresponding to HOMO → LUMO one-electron excitation in the synthesized compounds is ordered as follows: SBE > SBENi > SBECo. The relatively lower energy gap observed in SBECo suggests greater chemical reactivity and softness, making it more susceptible to electronic excitation. This reduced gap lifts-up the electron transfer from donor to acceptor regions, indicating higher polarizability and lower excitation energy requirements [34]. The 3D visualizations of the HOMO and LUMO for these synthesized compounds are illustrated in **Figure 11**.

3.8. Biological Studies

3.8.1. Evaluation of Antifungal Activity of Synthesized Compounds

The in vitro fungal resistant ability of synthesized ligand SBE and its metal complexes (SBECo and SBENi) was evaluated against Aspergillus niger and Fusarium oxysporum through poisoned food technique [35-38]. Freshly cultured fungal strains were utilized to evaluate the antifungal activity of the synthesized compounds. Stock solutions of each compound were prepared in DMSO, while Bavistin as a positive control, DMSO and water as negative controls. The compounds were incorporated to autoclaved(20 min, 125 °C) Malt Extract Agar(MEA) media(36 g/L) to obtain the final concentrations of 500 μg/ml (A), 250 μg/ml (B), and 125 μg/ml (C). Control plates containing only DMSO and water in MEA were also prepared. The medium was poured into a set of Petri plates in a laminar flow hood, as the media in the Petri plates solidified, 2.5 mm mycelial disc from actively grown fungal cultures were inoculated at the centre of each plate. Further on, these plates were incubated at 28 ℃ for eight days, and antifungal activity was assessed by measuring the reduction in mycelial growth compared to controls [39,40].

The results showed concentration-dependent antifungal activity. The antifungal assay results were evaluated by measuring the reduction in fungal colony diameter and calculating the percentage growth inhibition compared to controls. Notably, both the ligand and its metal complexes exhibited antifungal activity that increased with concentration, meaning higher antifungal effects were seen at higher concentrations of the ligand and complexes.

Among all tested compounds, the ligand SBE demonstrated relatively better fungal resistance than the metal complexes. At a concentration of 500 μg/ml of SBE, mycelium growth was minimal—with scanty spore germination—while at 125 μg/ml, some spores were present. The biological activities of these metal complexes are likely influenced by various factors, such as the specific metal ion, the ligand's structure, the stability of the chelated complexes, the ease of bond cleavage between the metal ion and the ligand, and others. These factors can affect how the compound's active sites interact with the target sites within the fungal cell.

The effectiveness of some therapeutic agents can often be improved by the presence of electron-withdrawing groups and ligands that coordinate with suitable metal ions. Some metal ions penetrate fungal cells and inactivate enzymes, or they can generate hydrogen peroxide or reactive oxygen species (ROS), leading to a lethal effect. Any chemotherapeutic used against fungi acts primarily in a fungistatic manner. Resistance to OTC drugs is a major worldwide issue concerning fungal diseases. In this study, in-vitro tests were conducted to examine the antifungal effects of the new Schiff base ligand SBE and its metal complexes SBECo and SBENi against two fungal strains, Aspergillus niger (**Figure 12 & 13)** and Fusarium oxysporum (**Figure 14 & 15**). The reduction in fungal colony diameter across different treatments and the control made comparisons straightforward.

It was observed that the SBE ligand, which contains active, electronically rich azomethine nitrogen and hydroxyl oxygen groups, enhances its ability to interact with fungal components, making it more effective than its metal complexes (which have reduced electron density). The biological activities observed also correlate with DFT data. According to DFT calculations, a lower dipole moment combined with a higher global nucleophilicity index indicates stronger biological activity for the SBE ligand. When the ligand chelates with metal ions, electron density shifts toward the metal, creating less polar or electronically deficient interaction sites, which explains why the metal complexes are generally less effective in resisting fungi.

Consequently, against A. niger, it was found that the ligand showed better antifungal activity than the metal complexes, although it was still less effective than the positive control, Bavistin. The order of antifungal activity against A. niger was: Bavistin (positive control) > SBE > SBECo > SBENi > negative controls (DMSO > Water) (**Table 10**). Similarly, for F. oxysporum, the ligand again was the most effective among the tested compounds but remained less potent than Bavistin. The resistance order against F. oxysporum was: Bavistin > SBE > SBENi > SBECo > negative controls (DMSO > Water) (**Table 11**).

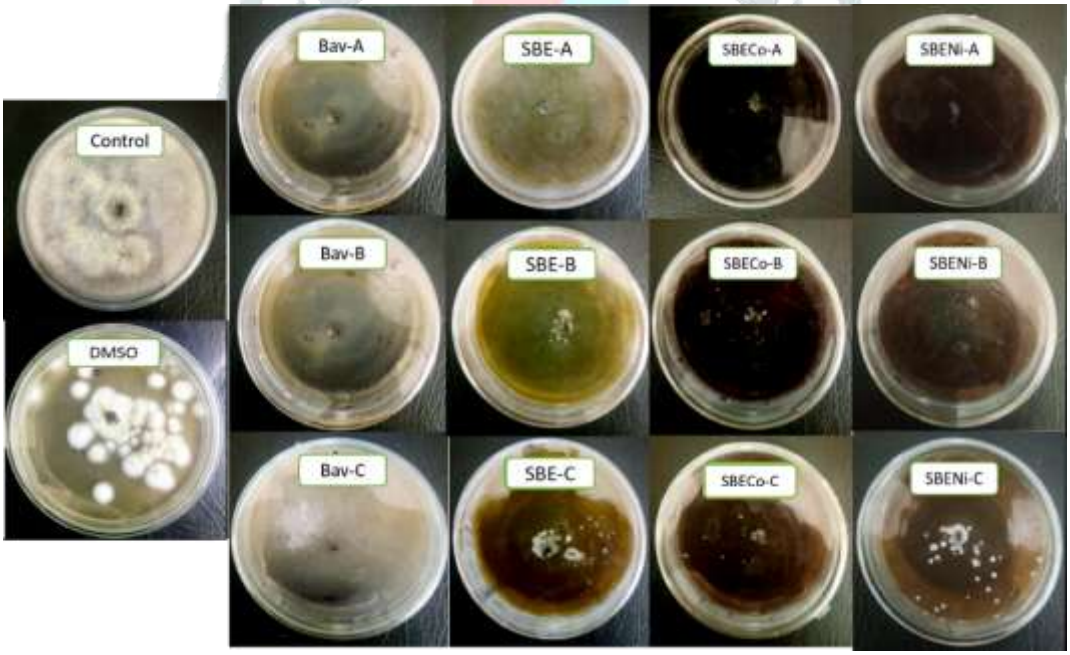

Figure 12: Pictorial representation of antifungal activity against Aspergillus niger treated with SBE ligand, its metal complexes, and controls at 500 µg/mL (A), 250 µg/mL (B), and 125 µg/mL (C)

Table 10: Antifungal assays representing percentage growth inhibition and mean fungal growth(mm) of Aspergillus niger by newly synthesized compounds and control agents at 500 µg/mL (A), 250 µg/mL (B) and 125 µg/mL (C) concentrations

Compounds	Aspergillus niger					
	Growth Inhibition (%)			Mean Fungal Growth (mm)		
	A	B	C	A	B	C
Control	5.76	5.76	5.76	90	90.0	90.0
DMSO	66.28	66.28	66.28	32.2	32.2	32.2
Bavistin	94.55	94.24	93.92	5.2	5.5	5.8
SBE	89.32	88.90	87.12	10.2	10.6	12.3
SBECo	87.43	86.18	83.98	12	13.2	15.3
SBENi	85.76	85.23	83.56	13.6	14.1	15.7

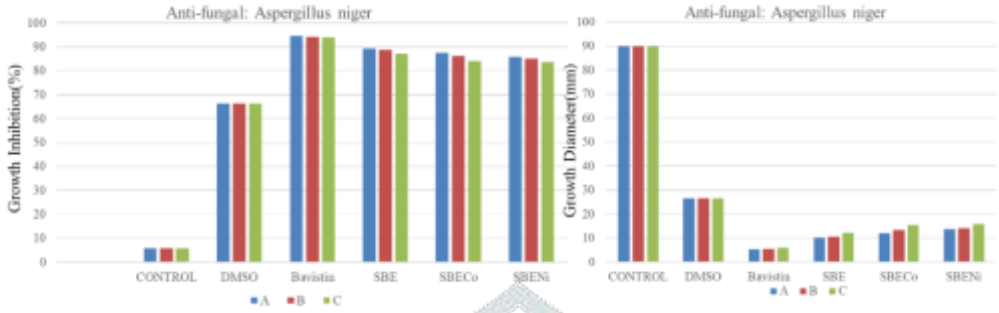

Figure 13: Graphical representation of % growth inhibition and mean mycelial diameter (mm) of Aspergillus niger treated with synthesized compounds and controls at 500 µg/mL (A), 250 µg/mL (B), and 125 µg/mL (C)

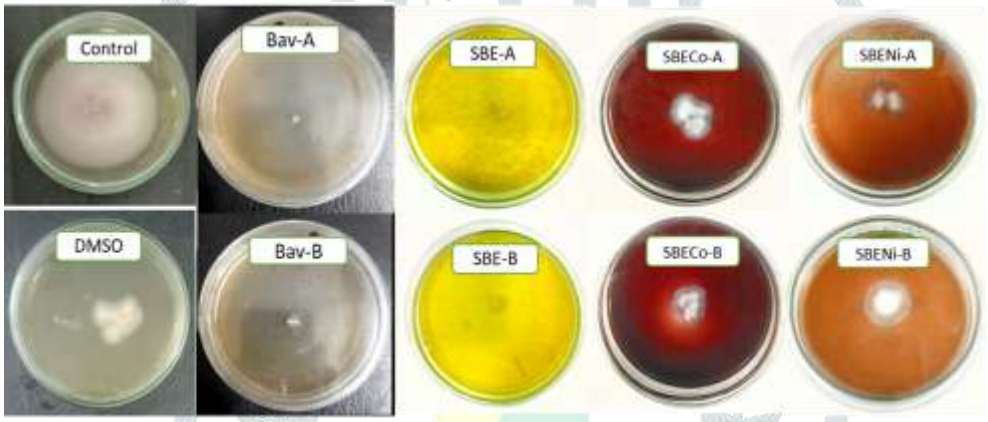

Figure 14: Pictorial description of Antifungal Activity of Synthesized Compounds Against F. oxysporum at 500 µg/mL (A) , and 250 µg/mL (B) Concentrations.

Table 11: Antifungal assays representing percentage growth inhibition and mean fungal growth(mm) of *Fusarium oxysporum* by newly synthesized compounds and control agents at 500 µg/mL (A), and 250 µg/mL (B) concentrations.

Compounds	Fusarium oxysporum			
	Growth Inhibition (%)		**Mean Fungal Growth (mm)**	
	A	**B**	**A**	**B**
Control	1.54	1.54	65.0	65.0
DMSO	56.92	56.92	28.0	28.0
Bavistin	92.30	92.00	5.0	5.2
SBE	87.69	84.61	8.0	10.0
SBECo	72.31	61.53	18.0	25.0
SBENi	69.23	61.54	20.0	25.0

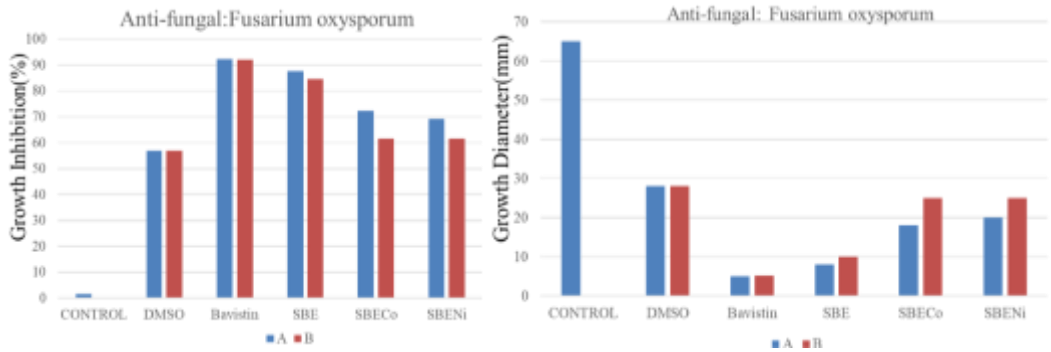

Figure 15: Graphical representation of % growth inhibition and mean fungal growth diameter(mm) of Fusarium oxysporum treated with synthesized compounds and controls in 500 μg/ml (A), 250 μg/ml (B) and 125 μg/ml concentrations.

3.9.2. Evaluation of Photocatalytic Dye Degradation Efficiency

The dye degradation potential of the synthesized ligand (SBE) and its metal complexes to degrade methylene blue (MB) dye under ultraviolet (UV) light was carefully studied. UV–Vis absorption spectra taken over time (**Figure 16**) tracked changes in MB dye concentration in both the presence and absence (control) of these compounds. Additionally, the percentage of dye degradation over time is shown in **Figure 17**, with final degradation results after 200 minutes summarized in **Table 12**.

Notably, a substantial decrease in the absorption peak at 664 nm (the λmax for MB dye) [41], along with a visible color change from deep blue to light greenish-blue, was observed with the nickel complex (SBENi). This indicates that SBENi had the greatest ability to adsorb and degrade the dye compared to other synthesized compounds. Conversely, the free ligand (SBE) showed the weakest adsorption performance.

The overall dye removal effectiveness followed the order: SBENi > SBECo > SBE > MB dye (control). This trend aligns with electron affinity values obtained from density functional theory (DFT) calculations, implying that the electronic properties of these compounds are key to their dye removal efficiency.

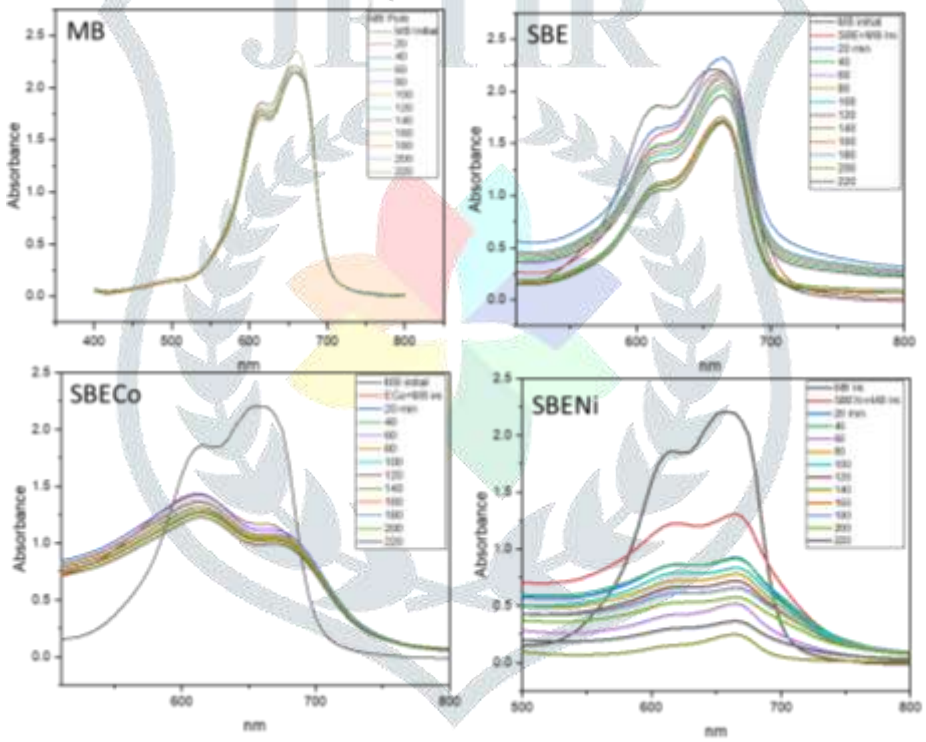

Figure 16: Time-dependent changes in absorption spectra of Methylene blue in the presence of UV light and synthesized compounds (0–200 min)

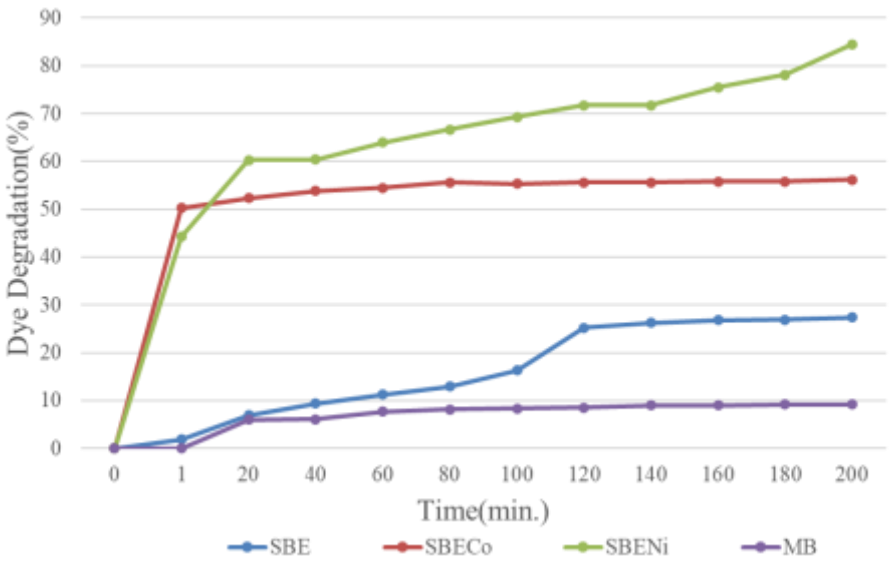

Figure 17: Comparative analysis of Methylene blue photodegradation rates under UV irradiation using synthesized compounds.

Table 12: UV-induced photodegradation of Methylene blue by SBE ligand and its metal complexes after 200 minutes.

Samples	Time	% Dye degradation
MB	200 min	9.53
SBE	200 min	27.5
SBECo	200 min	57.5
SBENi	200 min	89.2

4. Conclusion

A novel Schiff base ligand, 6,6'-((1,2-Diphenylethane-1,2-diylidene)bis(azaneylylidene))bis(4-chloro-3-nitrophenol) (SBE), along with its metal complexes SBECo, and SBENi, were synthesized utilizing the reflux method. The anticipated structural integrity and physicochemical properties of both the ligand and its metal complexes were confirmed through various analytical techniques, namely UV-Vis, FT-IR, 1H-NMR, mass spectrometry, P-XRD, and thermogravimetric analysis (thermal analysis). Moreover, Density Functional Theory (DFT) calculations, employing the B3LYP method with the appropriate basis set (6-31G for the ligand and LANL2DZ for the metal complexes), provided crucial insights into their optimized molecular geometries and electronic structures, strongly corroborating the experimental observations.

Beyond the fundamental aspects, the synthesized compounds demonstrated remarkable biological and environmental applications by showcasing the antifungal activity, and dye degradation capabilities. It was observed that the ligand SBE exhibited superior fungicidal when compared to the metal complexes. Regarding dye degradation potential, the SBENi metal complex exhibited a greater capacity to degrade methylene blue dye than the SBECo complexes and the ligand. These compelling findings emphasize the diverse applicability of this novel Schiff base ligand and its metal complexes, particularly in addressing biological and environmental challenges.

Notes

The authors declare no competing financial interest.

References:

[1] Juyal, Vijay Kumar, et al. "Schiff base metal complexes as a versatile catalyst: A review." *Journal of organometallic chemistry* 999 (2023): 122825.

[2] Cozzi, Pier Giorgio. "Metal–Salen Schiff base complexes in catalysis: practical aspects." *Chemical Society Reviews* 33.7 (2004): 410-421.

[3] Biswas, Tanya, et al. "Schiff bases: versatile mediators of medicinal and multifunctional advancements." *Letters in Organic Chemistry* 21.6 (2024): 505-519.

[4] Zhang, Wenbing, et al. "Nanosilica Schiff-Base Copper (II) complexes with sustainable antimicrobial activity against bacteria and reduced risk of harm to plant and environment." *ACS Sustainable Chemistry & Engineering* 5.1 (2017): 502-509.

[5] Chandra, Sulekh, and Suresh Kumar. "Synthesis, spectroscopic, anticancer, antibacterial and antifungal studies of Ni (II) and Cu (II) complexes with hydrazine carboxamide, 2-[3-methyl-2-thienyl methylene]." *Spectrochimica Acta Part A: Molecular and Biomolecular Spectroscopy* 135 (2015): 356-363.

[6] Boeckmann, Jan, and Christian Näther. "Solid-state transformation of [Co (NCS) 2 (pyridine) 4] into [Co (NCS) 2 (pyridine) 2] n: from Curie–Weiss paramagnetism to single chain magnetic behaviour." *Dalton Transactions* 39.45 (2010): 11019-11026.

[7] Boeckmann, Jan, and Christian Näther. "Solid-state transformation of [Co (NCS) 2 (pyridine) 4] into [Co (NCS) 2 (pyridine) 2] n: from Curie–Weiss paramagnetism to single chain magnetic behaviour." *Dalton Transactions* 39.45 (2010): 11019-11026.

[8] El-Gammal, Ola A., et al. "Structural characterization and biological activity of a new metal complexes based of Schiff base." *Journal of Molecular Liquids* 330 (2021): 115522.

[9] Islam, Mohammad Shahidul, et al. "Synthesis, molecular docking and enzyme inhibitory approaches of some new chalcones engrafted pyrazole as potential antialzheimer, antidiabetic and antioxidant agents." *Journal of Molecular Structure* 1269 (2022): 133843.

[10] Mahmoud, Nelly H., et al. "Spectroscopic studies, DFT calculations, cytotoxicity activity, and docking stimulation of novel metal complexes of Schiff base ligand of isonicotinohydrazide derivative." *Applied Organometallic Chemistry* 36.7 (2022): e6697.

[11] Hashem, Heba E., et al. "New heterocyclic Schiff base-metal complex: Synthesis, characterization, density functional theory study, and antimicrobial evaluation." *Applied Organometallic Chemistry* 35.9 (2021): e6322.

[12] Hassan, Ali M., et al. "Green synthesis, characterization, antimicrobial and anticancer screening of new metal complexes incorporating Schiff base." *ACS omega* 7.36 (2022): 32418-32431.

[13] Pola, Someshwar, et al. "Synthesis of new fused heterocyclic aromatic hydrocarbons via C–S and C–C bond formation by C–H bond activation in the presence of new Pd (ii) Schiff's base complexes." *RSC Advances* 6.91 (2016): 88321-88331.

[14] Saranya, Jagadeesan, et al. "Tetradentate Schiff base complexes of transition metals for antimicrobial activity." *Arabian Journal for Science and Engineering* 45.6 (2020): 4683-4695.

[15] Kalaycıoğlu, Zeynep, et al. "Efficient photocatalytic degradation of methylene blue dye from aqueous solution with cerium oxide nanoparticles and graphene oxide-doped polyacrylamide." *ACS omega* 8.14 (2023): 13004-13015.

[16] Arshad, Adil Hussain, et al. "MXene and MXene-based hybrid materials for pharmaceutical-induced pollutants removal via adsorption and photocatalysis: A critical viewpoint." *Environmental Technology Reviews* 14.1 (2025): 142-190.

[17] Din, Muhammad Imran, et al. "Fundamentals and photocatalysis of methylene blue dye using various nanocatalytic assemblies-a critical review." *Journal of Cleaner Production* 298 (2021): 126567.
[18] Kalaycıoğlu, Zeynep, et al. "Efficient photocatalytic degradation of methylene blue dye from aqueous solution with cerium oxide nanoparticles and graphene oxide-doped polyacrylamide." *ACS omega* 8.14 (2023): 13004-13015.
[19] Kumar, Hemant, and Ekta. "Photocatalytic degradation of naphthol blue black dye by Schiff base metal complex under UV light irradiation." *AIP Conference Proceedings*. Vol. 2352. No. 1. AIP Publishing LLC, 2021.
[20] Ejiah, Felicia Ndidi, et al. "Schiff bases as analytical tools: synthesis, chemo-sensor, and computational studies of 2-aminophenol Schiff bases." *Materials Advances* 4.10 (2023): 2308-2321.
[21] Tahmasbi, Ayub, Akbar Jafari, and Abbas Nikoo. "Synthesis, characterization, and nonlinear optical properties of copper (II) ligand Schiff base complexes derived from 3-Nitrobenzohydrazide and benzyl." *Scientific Reports* 13.1 (2023): 10988.
[22] Kasim, Mohamed Subarkhan Mohamed, Saranya Sundar, and Ramesh Rengan. "Synthesis and structure of new binuclear ruthenium (II) arene benzil bis (benzoylhydrazone) complexes: investigation on antiproliferative activity and apoptosis induction." *Inorganic chemistry frontiers* 5.3 (2018): 585-596.
[23] Nath, Mala, and Pramendra K. Saini. "Chemistry and applications of organotin (IV) complexes of Schiff bases." *Dalton Transactions* 40.27 (2011): 7077-7121.
[24] Shakir, Mohammad, et al. "Synthesis, spectroscopic characterization, DNA interaction and antibacterial study of metal complexes of tetraazamacrocyclic Schiff base." *Spectrochimica Acta Part A: Molecular and Biomolecular Spectroscopy* 93 (2012): 354-362.
[25] Kumar, TM Sharan, et al. "Novel Schiff base cobalt (ii) phthalocyanine with appliance of MWCNTs on GCE: enhanced electrocatalytic activity behaviour of α-amino acids." *RSC advances* 11.27 (2021): 16736-16746.
[26] Mohamed, Gehad G., et al. "Preparation, characterization and biological activity of novel metal-NNNN donor Schiff base complexes." *Spectrochimica Acta Part A: Molecular and Biomolecular Spectroscopy* 75.2 (2010): 678-685.
[27] El-Sonbati, A. Z., et al. "Synthesis, characterization of Schiff base metal complexes and their biological investigation." *Applied Organometallic Chemistry* 33.9 (2019): e5048.
[28] Abdel-Kader, Nora S., et al. "A coumarin Schiff base and its Ag (i) and Cu (ii) complexes: synthesis, characterization, DFT calculations and biological applications." *New Journal of Chemistry* 45.17 (2021): 7714-7730.
[29] Ghosh, Pushpal, et al. "Size of the rare-earth ions: a key factor in phase tuning and morphology control of binary and ternary rare-earth fluoride materials." *RSC advances* 7.53 (2017): 33467-33476.
[30] Gökce, Halil, and Semiha Bahçeli. "FT-IR, Micro-Raman and UV–vis spectroscopic and quantum chemical investigations of free 2, 2′-dithiodipyridine and its metal (Co, Cu and C) halide complexes." *Spectrochimica Acta Part A: Molecular and Biomolecular Spectroscopy* 114 (2013): 61-73.
[31] Alaşalvar, Can, et al. "Crystal structure and DFT calculations of 5-(4-Chlorophenyl)-1-(6-methoxypyridazin-3-yl)-1H-pyrazole-3-carboxylic acid." *Spectrochimica Acta Part A: Molecular and Biomolecular Spectroscopy* 132 (2014): 555-562.
[32] Sánchez-Márquez, Jesús, et al. "Local reactivity descriptors of the important atoms in chelotropic reactions provide insight into their global variants along the reaction path." *International Journal of Quantum Chemistry* 123.15 (2023): e27129.
[33] Venkatesh, G., et al. "Structural, electronic and optical properties of 2, 5-dichloro-p-xylene: experimental and theoretical calculations using DFT method." *RSC advances* 7.3 (2017): 1401-1412.
[34] Ani, Friday E., et al. "Crystal, spectroscopic and quantum mechanics studies of Schiff bases derived from 4-nitrocinnamaldehyde." *Scientific reports* 11.1 (2021): 8151.
[35] Varshney, Anshita, and A. P. Mishra. "Synthesis, spectral characterization, computational studies, antifungal, DNA interaction, antioxidant and fluorescence property of novel Schiff base ligand and its metal chelates." *Spectrochimica Acta Part A: Molecular and Biomolecular Spectroscopy* 297 (2023): 122765.
[36] Varshney, Anshita, et al. ”Novel Schiff base ligand and its Co(II) & Cu(II) Metal complexes: Synthesis, Physicochemical Characterization, DNA Binding, and Antifungal Screening. Mediterranean Journal of Chemistry, Vol. 13 No. 3 (2023). DOI: 10.13171/mjc02306071707vashney
[37] Choubey, A. K., and A. P. Mishra. “New Bioactive Ligand and Its Ni(II) and Cu(II) Complexes: Synthetic Preparation, Spectroscopic Characterization and Biological Evaluation.” Mediterranean Journal of Chemistry, Vol. 15No. 2 (2025). DOI: https://doi.org/10.13171/mjc025040081830choubey
[38] Elsayed, Shadia A., et al. "Novel metal complexes of 3-acetylcoumarin-2-hydrazinobenzothiazole Schiff base: Design, structural characterizations, DNA binding, DFT calculations, molecular docking and biological studies." *Applied Organometallic Chemistry* 34.6 (2020): e5643.
[39] Chandra, Sulekh. "Synthesis, spectroscopic characterization, molecular modeling and antimicrobial activities of Mn (II), Co (II), Ni (II), Cu (II) complexes containing the tetradentate aza Schiff base ligand." *Spectrochimica Acta Part A: Molecular and Biomolecular Spectroscopy* 103 (2013): 338-348.
[40] Mangamamba, T., M. C. Ganorkar, and G. Swarnabala. "Characterization of complexes synthesized using Schiff base ligands and their screening for toxicity two fungal and one bacterial species on rice pathogens." *International Journal of Inorganic Chemistry* 2014.1 (2014): 736538.
[41] Chen, Jiansong, et al. "Facile synthesis of lignin Schiff base-copper complex as a catalyst for methylene blue and 4-nitrophenol removal." *Industrial crops and products* 206 (2023): 117627.